Physica D 341 (2017) 45–59

Contents lists available at ScienceDirect

Physica D

journal homepage: www.elsevier.com/locate/physd

A theory of synchrony for active compartments with delays coupled through bulk diffusion

Bin Xu, Paul C. Bressloff*

Department of Mathematics, University of Utah, Salt Lake City, UT 84112, USA

ARTICLE INFO

Article history:
Received 5 May 2016
Accepted 3 October 2016
Available online 7 October 2016
Communicated by K. Josic

Keywords:
Diffusion
Delay differential equations
Hopf bifurcation

ABSTRACT

We extend recent work on the analysis of synchronization in a pair of biochemical oscillators coupled by linear bulk diffusion, in order to explore the effects of discrete delays. More specifically, we consider two well-mixed, identical compartments located at either end of a bounded, one-dimensional domain. The compartments can exchange signaling molecules with the bulk domain, within which the signaling molecules undergo diffusion. The concentration of signaling molecules in each compartment is modeled by a delay differential equation (DDE), while the concentration in the bulk medium is modeled by a partial differential equation (PDE) for diffusion. Coupling in the resulting PDE–DDE system is via flux terms at the boundaries. Using linear stability analysis, numerical simulations and bifurcation analysis, we investigate the effect of diffusion on the onset of a supercritical Hopf bifurcation. The direction of the Hopf bifurcation is determined by numerical simulations and a winding number argument. Near a Hopf bifurcation point, we find that there are oscillations with two possible modes: in-phase and anti-phase. Moreover, the critical delay for oscillations to occur increases with the diffusion coefficient. Our numerical results suggest that the selection of the in-phase or anti-phase oscillation is sensitive to the diffusion coefficient, time delay and coupling strength. For slow diffusion and weak coupling both modes can coexist, while for fast diffusion and strong coupling, only one of the modes is dominant, depending on the explicit choice of DDE.

1. Introduction

Recently, a class of compartmental model of synchronized biochemical oscillators coupled by bulk diffusion has been analyzed by Gou et al. [1–4] and Sancho et al. [5]. Specifically, the models in [1–4] consider two or more well mixed identical compartments and a bulk medium between the compartments where signaling molecules undergo diffusion. The concentration of signaling molecules within each compartment is modeled by a system of nonlinear ordinary differential equations (ODEs) while the concentration in the bulk medium is modeled by a partial differential equation (PDE) for diffusion and degradation. Gou et al. assume that each isolated compartment is a conditional oscillator. That is, in isolation a compartment's dynamics is at a stable fixed point, but can exhibit sustained oscillations in a different parameter regime. Each isolated compartment is modeled in terms of a planar dynamical system without delays. Using linear stability analysis, the authors showed that diffusive coupling can induce in-phase or anti-phase oscillations for a pair of active compartments. One application of this type of PDE–ODE model is to intercellular signaling mechanisms such as quorum sensing, where each compartment is a microbial cell and the bulk is the extracellular medium between cells [6–11]. Quorum sensing involves the production and extracellular secretion of certain signaling molecules called *autoinducers*. Each cell also has receptors that can specifically detect the signaling molecule via ligand–receptor binding, which then activates transcription of certain genes, including those for inducer synthesis. However, since there is a low likelihood of an individual bacterium detecting its own secreted inducer, the cell must encounter signaling molecules secreted by other cells in its environment in order for gene transcription to be activated. When the cell density is low, diffusion reduces the concentration of the inducer in the surrounding medium to almost zero, resulting in small amounts of inducer being produced. On the other hand, as the population grows, the concentration of the inducer passes a threshold, causing more inducer to be synthesized. This generates a positive feedback loop that fully activates the receptor, and induces the up-regulation of other specific genes. Hence, all of the cells initiate

* Corresponding author.
E-mail addresses: xu@math.utah.edu (B. Xu), bresslof@math.utah.edu (P.C. Bressloff).

http://dx.doi.org/10.1016/j.physd.2016.10.001
0167-2789/

transcription at approximately the same time, resulting in some form of coordinated behavior such as synchronized oscillations.

PDE–ODE models can also be applied at the single cell level [12], with each compartment a dynamically active membrane and the bulk domain corresponding to the cytoplasm. In many cases, a complicated multi-step chemical reaction within the membrane can be reduced to a simpler single-step model with discrete delays, see Refs. [13,14]. This motivates the current study, namely, to investigate the effects of bulk diffusive coupling on the synchronization of a pair of biochemical compartments evolving according to a delay-differential equation (DDE) rather than a planar ODE. For concreteness, we focus on a pair of delayed logistic equations coupled by bulk diffusion, but establish that similar results hold for another classical DDE, namely, the Mackey–Glass equation [15]. Although the delayed logistic equation has been well studied (see [16–20]), there has been relatively little work on the interaction of time delays and diffusion under the framework of PDE–DDE models. One notable exception concerns a PDE–DDE model of genetic control [21–23]. These authors model the concentration of mRNA and a repressor protein in two compartments: a well-mixed compartment (the nucleus) where mRNA is produced and the cell cytoplasm where ribosomes are randomly dispersed and translation occurs. In this paper, we follow the PDE–ODE framework of Gou et al. [1–4] by considering diffusive coupling between two well mixed compartments whose intrinsic reaction dynamics includes a time delay. In particular, we explore how diffusion affects the critical time delay for a Hopf bifurcation and the nature of oscillatory solutions in the parameter region above the Hopf bifurcation point. In contrast to a single, well-mixed compartment, one has to distinguish between in-phase and anti-phase oscillatory modes along the lines of Gou et al. [1–3]. Note that one other major difference between the PDE–ODE models of Gou et al. and our PDE–DDE model is that we do not include a degradation term within the bulk diffusion equation. This is a reasonable approximation if the degradation time is much longer than the typical time delay. Moreover, our main interest in this paper is how diffusion affects oscillations that already exist in the absence of diffusion, rather than exploring diffusion-induced oscillations; the latter appear to require non-zero degradation rates [1–3]. A more pragmatic reason for ignoring degradation is that the introduction of a delay introduces another time-scale into the system, and we want to restrict the number of parameters that we vary.

The paper is organized as follows. In Section 2, we introduce the one-dimensional PDE–DDE model for the delayed logistic equation. We then use linear stability analysis to derive a characteristic equation that depends nonlinearly on the associated eigenvalue. We use the characteristic equation to derive necessary conditions for a Hopf bifurcation. We then numerically calculate the critical time delay as a function of various model parameters, including the time delay, the bulk diffusivity and the strength of diffusive coupling at the boundaries. We plot Hopf bifurcation curves as a function of these different parameters, and then use numerical simulations to explore the switching between in-phase and anti-phase oscillations with changes in parameters (Section 3). We also use the bifurcation tool DDE-BIFTOOL [24] to plot the amplitude of the periodic solutions. One limitation of our linear stability analysis is that we do not check that the pair of pure imaginary eigenvalues crosses over to the right-half complex plane above the Hopf bifurcation point, nor determine whether or not there are already other eigenvalues in the right-half complex plane. Therefore, in Section 4 we apply the winding number method to detect the number of eigenvalues in the right-half plane for different parameter regimes. In Section 5, we briefly explore extensions of our analysis to (i) asymmetric coupling and (ii) a PDE–DDE model based on the Mackey–Glass equation [15].

Note that the PDE–DDE model considered in this paper is distinct from our recent model of cell polarization in fission yeast [25]. The latter model describes bulk diffusion of a signaling molecule Rho GTPase Cdc42 in the cytoplasm, which is coupled to a pair of delay differential equations (DDEs) at the ends of the cell via boundary conditions. The latter represent the binding of Cdc42 to the cell membrane and re-release into the cytoplasm via unbinding. The nontrivial nature of the dynamics arises from the fact that both the binding and unbinding rates at each end are taken to depend nonlinearly on the local membrane concentration of Cdc42. In particular, the association rate is regulated by positive feedback and the dissociation rate is regulated by delayed negative feedback. From a mathematical perspective, the fission yeast model differs from our current PDE–DDE model, since in the former case each compartment does not have its own intrinsic dynamics, rather it is solely driven by the diffusive flux into the compartment.

2. Oscillations in a PDE–Logistic model

Consider the concentration of a single chemical species in a one-dimensional finite domain $[0, L]$. The boundaries $x = 0$ and $x = L$ represent dynamically active membrane whose dynamics is governed by a DDE. For concreteness, we take the DDE to be the delayed logistic equation; we consider the Mackey–Glass DDE in Section 5. The bulk region $(0, L)$ represents the cytoplasm of a cell within which molecules undergo diffusion with diffusion coefficient D. The bulk region and the two end compartments are coupled by a linear diffusive flux with coupling parameter β. Denoting the concentration at the boundaries as $X_1(t), X_2(t)$ and the concentration in the bulk as $C(x, t)$, the model is given by

$$\begin{aligned} &\frac{\partial C}{\partial t}(x,t) = D\frac{\partial^2 C}{\partial x^2}, \quad 0 < x < L,\ t > 0\\ &D\partial_x C(0,t) = \beta(C(0,t) - X_1(t)),\\ &-D\partial_x C(L,t) = \beta(C(L,t) - X_2(t)) \end{aligned} \tag{1}$$

and

$$\frac{dX_1}{dt} = \beta(C(0,t) - X_1(t)) + f(X_1(t), X_1(t-\tau)), \tag{2a}$$

$$\frac{dX_2}{dt} = \beta(C(L,t) - X_2(t)) + f(X_2(t), X_2(t-\tau)) \tag{2b}$$

where

$$f(x(t), x(t-\tau)) = rx(t)(1 - x(t-\tau)/M). \tag{3}$$

Here τ is the time delay, r is the growth rate and M is the carrying capacity.

A steady-state solution of the above PDE–DDE satisfies

$$\begin{aligned} &C(x) = \frac{C_L - C_0}{L}x + C_0,\\ &D\frac{C_L - C_0}{L} = \beta(C_0 - X_1) = -\beta(C_L - X_2). \end{aligned} \tag{4}$$

Rewriting C_0 and C_L in terms of X_1 and X_2 gives

$$C_0 = \frac{(1+\alpha)X_1 + \alpha X_2}{1+2\alpha}, \qquad C_L = \frac{\alpha X_1 + (1+\alpha)X_2}{1+2\alpha},$$

with $\alpha = D/(L\beta)$. It follows that

$$C_0 - X_1 = \frac{\alpha(X_2 - X_1)}{1+2\alpha}, \qquad C_L - X_2 = \frac{\alpha(X_1 - X_2)}{1+2\alpha}. \tag{5}$$

Suppose $X_1 > X_2$, then $C_0 - X_1 < 0$ and $C_L - X_2 > 0$. Thus $f(X_1, X_1) = -\beta(C_0 - X_1) > 0$. Hence $0 < X_1 < M$. Similarly, we have $f(X_2, X_2) = -\beta(C_L - X_2) < 0$. Hence $X_2 < 0$ or $X_2 > M$. Since $X_1 > X_2$, we have $X_2 < 0$. This implies that any nonnegative

steady state solution (X_1, X_2) must satisfy $X_1 = X_2$. It then follows that

$$C(x) = C_0 = X_1 = X_2, \qquad f(X_1, X_1) = 0.$$

The function $F(x) = f(x, x)$ has a trivial root at $x = 0$, which is unstable, and a positive root at $x = M$.

2.1. Linear stability analysis

We will investigate the occurrence of oscillations in the PDE–Logistic model by carrying out a linear stability analysis of the positive steady state,

$$C(x) = C_0 = X_1, \quad X_1 = X_2 = M,$$

and deriving conditions for a Hopf bifurcation. An investigation of linear stability means that we want to determine the spectrum of the linear operators obtained by linearizing about the fixed point. Therefore, we consider perturbed solutions of the form

$$C(x) = C_0 + \mathrm{e}^{\lambda t}\eta(x), \qquad X_i = M + \phi_i \mathrm{e}^{\lambda t}, \quad i = 1, 2.$$

The condition for linear stability then reduces to the requirement that all eigenvalues λ have negative real part. Substituting into the linearized system near the steady state then gives

$$\begin{cases} D\eta''(x) = \lambda\eta(x), \\ D\eta'(0) = \beta(\eta(0) - \phi_1) \\ -D\eta'(L) = \beta(\eta(L) - \phi_2) \end{cases} \tag{6}$$

and

$$\begin{cases} \lambda\phi_1 = \beta(\eta(0) - \phi_1) - r\mathrm{e}^{-\lambda\tau}\phi_1 \\ \lambda\phi_2 = \beta(\eta(L) - \phi_2) - r\mathrm{e}^{-\lambda\tau}\phi_2. \end{cases} \tag{7}$$

Using Eq. (7), we can rewrite (ϕ_1, ϕ_2) in terms of $\eta(0)$ and $\eta(L)$. That is,

$$\phi_1 = \frac{\beta\eta(0)}{\lambda + \beta + r\mathrm{e}^{-\lambda\tau}}, \qquad \phi_2 = \frac{\beta\eta(L)}{\lambda + \beta + r\mathrm{e}^{-\lambda\tau}}. \tag{8}$$

Substituting it into the boundary conditions of $\eta(x)$ gives

$$\begin{cases} D\eta''(x) = \lambda\eta(x), \\ D\eta'(0) = B(\lambda, \tau)\eta(0) \\ -D\eta'(L) = B(\lambda, \tau)\eta(L) \end{cases} \tag{9}$$

where

$$B(\lambda, \tau) = \beta\left[1 - \frac{\beta}{\lambda + \beta + r\mathrm{e}^{-\lambda\tau}}\right]. \tag{10}$$

The eigenvector $\eta(x)$ can be expressed in the form

$$\eta(x) = \frac{\eta_0 + \eta_1}{2}\frac{\cosh\left(\sqrt{\lambda/D}\left(x - \frac{L}{2}\right)\right)}{\cosh\left(\sqrt{\lambda/D}\frac{L}{2}\right)} + \frac{\eta_1 - \eta_0}{2}\frac{\sinh\left(\sqrt{\lambda/D}\left(x - \frac{L}{2}\right)\right)}{\sinh\left(\sqrt{\lambda/D}\frac{L}{2}\right)}, \tag{11}$$

where η_0 and η_1 are unknown coefficients. The boundary conditions require

$$\begin{pmatrix} \mathcal{A}_+(\lambda) + B(\lambda, \tau) & \mathcal{A}_-(\lambda) \\ \mathcal{A}_-(\lambda) & \mathcal{A}_+(\lambda) + B(\lambda, \tau) \end{pmatrix}\begin{pmatrix} \eta_0 \\ \eta_1 \end{pmatrix} = 0 \tag{12}$$

where

$$\mathcal{A}_\pm(\lambda) = \frac{\sqrt{\lambda D}}{2}\left[\tanh\left(\frac{L}{2}\sqrt{\lambda/D}\right) \pm \coth\left(\frac{L}{2}\sqrt{\lambda/D}\right)\right].$$

Since the matrix in Eq. (12) is cyclic and symmetric, it follows that Eq. (12) has the solutions $\eta_0 = \eta_1 = 1$ (in-phase) and $\eta_0 = -\eta_1 = 1$ (anti-phase) with λ satisfying the corresponding pair of equations

$$B(\lambda, \tau) = -\sqrt{\lambda D}\tanh\left(\frac{L}{2}\sqrt{\frac{\lambda}{D}}\right) \quad \text{(in-phase)}, \tag{13a}$$

$$B(\lambda, \tau) = -\sqrt{\lambda D}\coth\left(\frac{L}{2}\sqrt{\frac{\lambda}{D}}\right) \quad \text{(anti-phase)}. \tag{13b}$$

Note that the presence of terms involving $\sqrt{\lambda/D}$ means that we have to introduce a branch cut in the complex λ-plane along $(-\infty, 0]$ with $-\pi < \mathrm{Arg}(\lambda) < \pi$. Fortunately, for finite D, L this does not affect the eigenvalue relation (13) since, as $\lambda \to 0$, we have $\tanh(\sqrt{\lambda/4D}) \to \sqrt{\lambda/4D}$ and $\coth(\sqrt{\lambda/4D}) \to \sqrt{4D/\lambda}$, that is, any square roots in (13) cancel. However, care has to be taken in the limit $D \to 0$, since one can no longer eliminate the square roots and there is a continuous spectrum in addition to a discrete spectrum. We will avoid these complexities here by taking $D > 0$.

We now use Eqs. (13) to derive necessary conditions for a Hopf bifurcation. That is, we look for pure imaginary solutions $\lambda = i\omega$ with ω real and construct Hopf bifurcation curves as a function of D, τ and β. Note, however, that in order to ensure the emergence of limit cycle oscillations via a primary Hopf bifurcation, one also has to check that a pair of eigenvalues cross over to the right-half complex plane as one crosses the Hopf curve and that there are no other eigenvalues already in the right-half plane. One way to keep track of the number of eigenvalues in the right-half complex plane is to use a winding number argument (see Section 4). One issue that cannot be addressed using linear stability analysis is whether or not a Hopf bifurcation is supercritical. However, all of our numerical simulations suggest that the bifurcation is indeed supercritical (see Section 3).

Although we take $D > 0$ throughout, we first briefly consider the discrete spectrum when $D \to 0$ for $\lambda \neq 0$. Noting that

$$\lim_{D\to 0}\sqrt{\lambda D}\tanh\left(\frac{L}{2}\sqrt{\frac{\lambda}{D}}\right) = \lim_{D\to 0}\sqrt{\lambda D}\coth\left(\frac{L}{2}\sqrt{\frac{\lambda}{D}}\right) = 0,$$

we have

$$B(\lambda, \tau) = \beta\left[1 - \frac{\beta}{\lambda + \beta + r\mathrm{e}^{-\lambda\tau}}\right] = 0.$$

It follows that

$$\lambda + r\mathrm{e}^{-\lambda\tau} = 0. \tag{14}$$

This is the characteristic equation of the delayed logistic equation

$$\frac{dx}{dt} = f(x(t), x(t-\tau)) = rx(t)(1 - x(t-\tau)/M).$$

At a Hopf bifurcation point, the critical time delay τ and the frequency ω satisfy

$$\cos(\omega\tau) = 0, \qquad \omega - r\sin(\omega\tau) = 0.$$

It follows that

$$\tau = \frac{\pi}{2r} + \frac{2n\pi}{r}, \qquad \omega = r > 0, \quad n = 0, 1, 2, \ldots \tag{15}$$

In the slow diffusion limit, the Hopf point occurs at $\tau = \pi/(2r)$, and is independent of the coupling parameter β. The diffusion is too slow to affect the concentration at the membrane.

Next, we consider the solution of Eq. (13) as $D \to \infty$. Assuming $|\lambda| = O(1) \ll D$, we have

$$\lim_{D\to\infty}\sqrt{\lambda D}\tanh\left(\frac{L}{2}\sqrt{\frac{\lambda}{D}}\right) = \frac{\lambda L}{2},$$

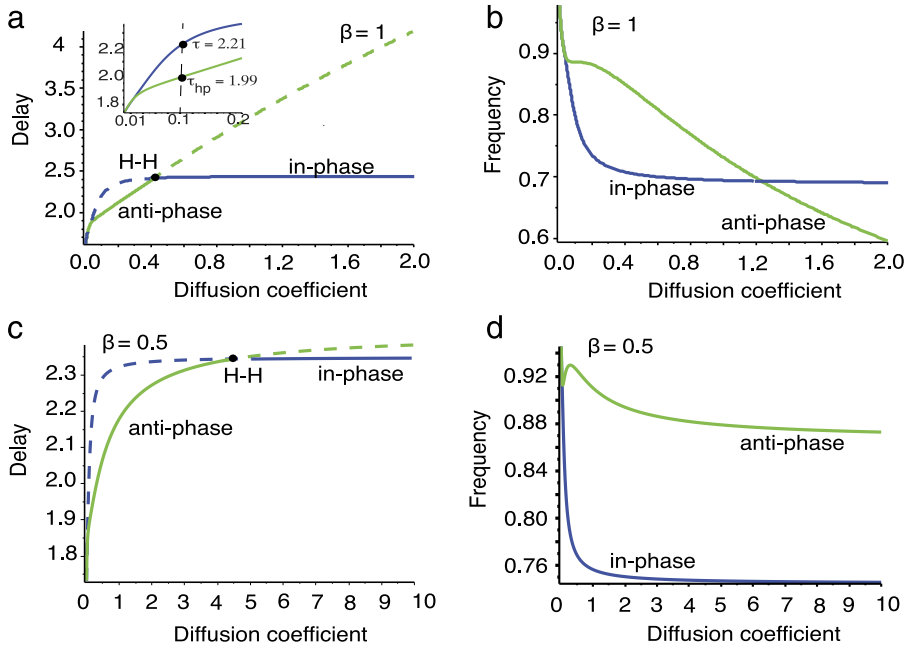

Fig. 1. Hopf bifurcation curves in (D, τ) plane for different values of the coupling parameter β. (a, c) Critical time delay τ_c vs. D with $\beta = 1, 0.5$, respectively. Solid curves show Hopf bifurcation points, whereas dashed curves are continuations through a double Hopf point (H–H). Below the primary branch, the steady state is stable. (b, d) Frequency ω (imaginary eigenvalue) vs. D with $\beta = 1, 0.5$, respectively. As D increases the primary bifurcation switches from an anti-phase to an in-phase limit cycle oscillation. Blue: in-phase. Green: anti-phase. Other parameters: $L = 1$, $r = 1$, $M = 1$. (For interpretation of the references to color in this figure legend, the reader is referred to the web version of this article.)

and

$$\sqrt{\lambda D}\coth\left(\frac{L}{2}\sqrt{\frac{\lambda}{D}}\right) \approx \frac{2D}{L} = O(D) \to \infty.$$

Hence the solution (τ, ω) of Eq. (13) in the fast diffusion limit satisfies

$$B(\lambda, \tau) = -\frac{\lambda L}{2}, \quad \text{or} \quad B(\lambda, \tau) = O(D) \to \infty. \tag{16}$$

The first equation in Eq. (16) gives the characteristic equation

$$\beta\left[1 - \frac{\beta}{\lambda + \beta + re^{-\lambda\tau}}\right] = -\frac{\lambda L}{2}. \tag{17}$$

Noting that for any $\lambda > 0$ real and $\tau > 0$,

$$1 - \frac{\beta}{\lambda + \beta + re^{-\lambda\tau}} > 0 > -\frac{\lambda L}{2\beta},$$

thus Eq. (17) has no positive real root. In fact, there is a negative real root. A Hopf bifurcation can occur as the eigenvalue crosses the imaginary axis. Setting $\lambda = i\omega$, the critical time delay and frequency at a Hopf point satisfy

$$1 + i\frac{\omega L}{2\beta} = \frac{\beta}{i\omega + \beta + re^{-i\omega\tau}} = \frac{\beta}{\beta + r\cos\omega\tau + i(\omega - r\sin(\omega\tau))}. \tag{18}$$

This equation can be solved numerically and the critical time delay is the same as the asymptote of the Hopf curve (in-phase) in Fig. 1(a).

The second equation in (16) does not have a solution unless

$$\lambda + \beta + re^{-\lambda\tau} = 0. \tag{19}$$

This type of characteristic equation has been studied in detail in [26,27]. Setting $\lambda = i\omega$, and taking $\omega > 0$ without loss of generality gives

$$\beta + r\cos\omega\tau = 0, \qquad \omega - r\sin\omega\tau = 0. \tag{20}$$

It follows that

$$\cos\omega\tau = -\frac{\beta}{r}, \qquad \omega = r\sin\omega\tau = \sqrt{r^2 - \beta^2}.$$

If $\beta > r$, there is no solution of (ω, τ). This implies that the critical time delay (associated with the anti-phase oscillation) does not exist for strong coupling β in the fast diffusion limit. On the other hand, if $\beta < r$, then there are denumerably many solutions

$$\omega = \sqrt{r^2 - \beta^2} > 0, \qquad \tau_n = \frac{(2n-1)\pi - \arccos(\beta/r)}{\omega},$$
$$n \in \mathbb{N}.$$

2.2. Hopf bifurcation curves

Using the above linear stability analysis, we now construct Hopf bifurcation curves with respect to different model parameters. In Fig. 1, Hopf bifurcation curves for the critical time delay τ_c are plotted as a function of the diffusion coefficient D for fixed coupling β. The critical time delay is computed by taking the real and imaginary parts of the two eigenvalue relations in (13) and solving the resulting system using Maple. There are two branches of Hopf curves corresponding to in-phase and anti-phase oscillations; they intersect at Hopf–Hopf points, which act as organizing centers for more complex oscillatory solutions. It is difficult to resolve which branch is dominant as $D \to 0$, since both the in-phase and anti-phase branches approach the critical time delay of the uncoupled delayed logistic equation. However, away from the origin, we find that as the diffusion coefficient D increases the critical time delay increases, and the primary bifurcation switches from an anti-phase to an in-phase oscillation. It can be checked that the asymptotic limit of the in-phase branch agrees with the solution $(\lambda, \tau) = (i\omega, \tau)$ of Eq. (17). In Fig. 2, we plot the corresponding Hopf bifurcation curves in the (β, τ) plane for fixed D Now there is a switch from anti-phase to in-phase oscillations as β is increased away from zero.

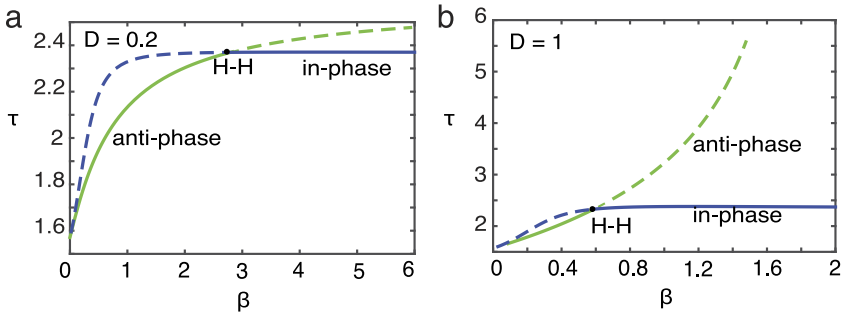

Fig. 2. Hopf bifurcation curves in (β, τ) plane for (a) $D = 0.2$ and (b) $D = 1$. Solid curves show Hopf bifurcation points, whereas dashed curves are continuations through a double Hopf point (H–H). Below the primary branch the steady-state solution is stable. As β increases the primary bifurcation switches from an anti-phase to an in-phase limit cycle oscillation. Blue: in-phase. Green: anti-phase. Other parameters: $L = 1$, $r = 1$, $M = 1$. (For interpretation of the references to color in this figure legend, the reader is referred to the web version of this article.)

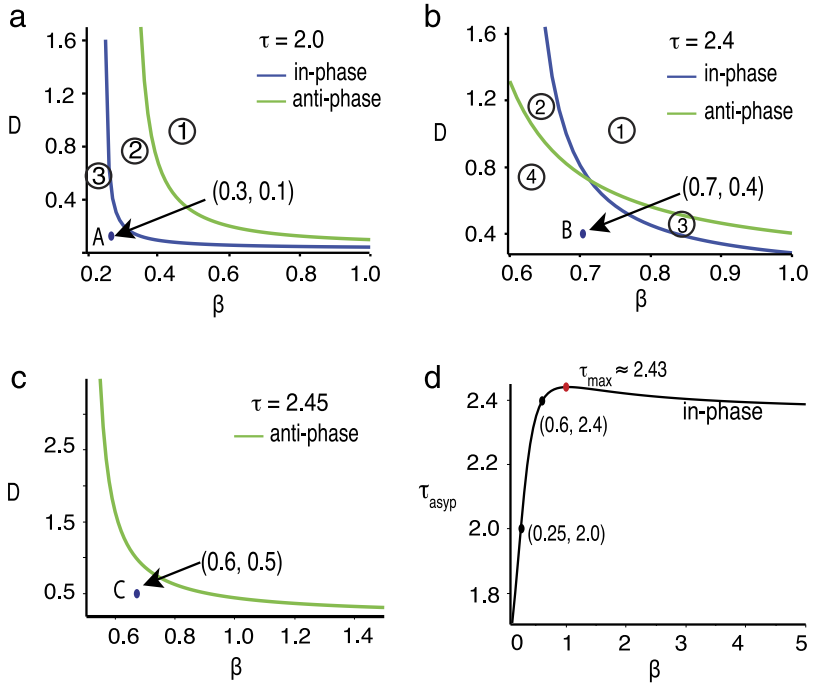

Fig. 3. Phase diagram in (D, τ) plane with different time delays. Anti-phase (in-phase) oscillations exist for (β, D) below the green (blue) line. (a) For $\tau = 2$, the steady-state is stable in region ①, and an anti-phase oscillation exists in regions ②. In region ③, both in-phase and anti-phase oscillations exist, however, numerical simulations suggest that the in-phase oscillation is unstable, see Fig. 4(a). (b) $\tau = 2.4$. The blue and green curves intersect. Our numerical plot in Fig. 4(b) suggests there is possibly an unstable torus bifurcation. (c) $\tau = 2.45$. Anti-phase oscillations exist for parameters below the green line. In-phase oscillations exist for any choice of (β, D). In the coexistence region, i.e., below the green line, we find that an in-phase oscillation can evolve to an anti-phase oscillation, see Fig. 4(c). (d) The asymptote of the critical time delay (solution of Eq. (18)) as a function of the coupling strength as $D \to \infty$. The two points $(\beta, \tau) = (0.25, 2.0)$ and $(0.6, 2.4)$ implies the asymptote of β for $\tau = 2, 2.4$, see Fig (a, b). (For interpretation of the references to color in this figure legend, the reader is referred to the web version of this article.)

Next, we take the time delay to be fixed and plot the phase diagram in the (β, D) plane, see Fig. 3. This is computed by numerically solving the eigenvalue Eq. (13) for the solution $\lambda = i\omega$ and D with a varying β. For $\tau = 2$, anti-phase (in-phase) oscillations exist for parameters below the green (blue) line. Above these lines, i.e., region ①, the steady state is stable. This indicates that for sufficiently large (β, D), the fixed time delay $\tau = 2$ is below a Hopf bifurcation. This result is consistent with the numerical results shown in Figs. 1 and 2. In the coexistence region ③, the in-phase oscillation is observed to be unstable, see Fig. 4(a). For $\tau = 2.4$, similar results are observed. However, one difference between $\tau = 2$ and $\tau = 2.4$ is that the blue and green curves intersect in the latter case. Numerical solutions for (β, D) chosen within the coexistence region shows there is a torus bifurcation, see Fig. 4(b). For $\tau = 2.45$, the time delay is sufficiently large so that in-phase oscillations exist for any (β, D). This can be explained by the plot of the asymptote of the critical time delay in the limit $D \to \infty$, which has a maximum around 2.43, see Fig. 3(d). On the other hand, anti-phase oscillations exist for parameters below the green line. Again, we find that the in-phase oscillation can lose its stability in the coexistence region, see Fig. 4(c).

In summary, our linear stability analysis suggests that the existence of oscillations depends on the diffusion coefficient, coupling strength and time delay. First, the critical time delay at a Hopf bifurcation increases as the diffusion coefficient or coupling strength increases. Second, for a fixed time delay, the effect of diffusion or coupling on the stability of steady state is sensitive to the value of the time delay. In particular, for a small time delay $(\tau < \pi/2)$, changing the diffusion coefficient or coupling strength will not destabilize the steady state. For a sufficiently large time delay, oscillations always exist for any (D, β). For a moderate time delay, decreasing the diffusion coefficient or coupling strength can give rise to in-phase or anti-phase oscillations.

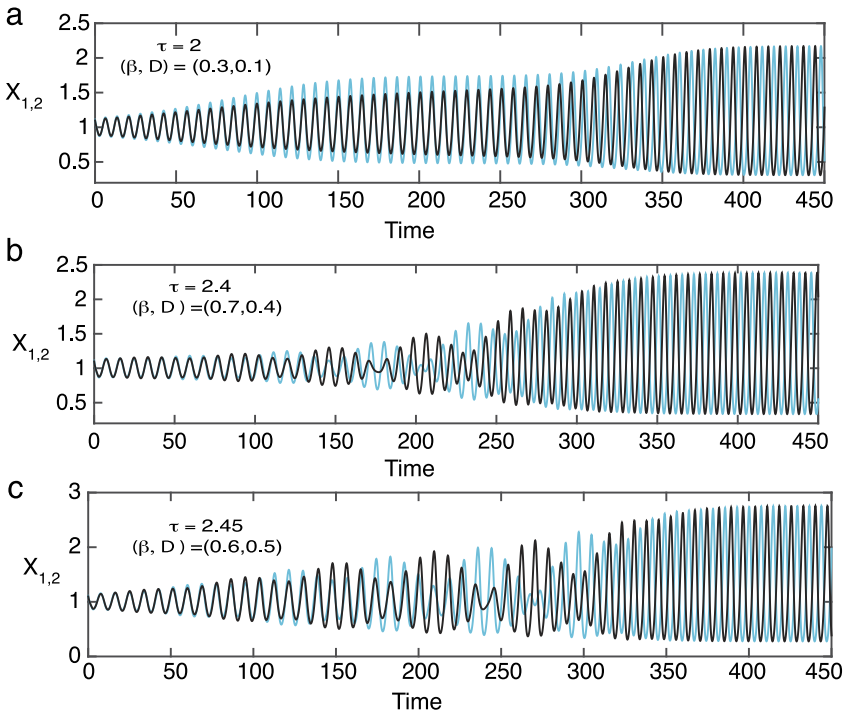

Fig. 4. Instability of the in-phase oscillation in the coexistence region corresponding to points A, B, C, respectively, in Fig. 3(a)–(c). Initial condition: $C(x, 0) = 1$, $X_1(0) = 1.1$, $X_2(0) = 1.11$. (For interpretation of the references to color in this figure legend, the reader is referred to the web version of this article.)

3. In-phase vs. anti-phase oscillations

In this section, we numerically explore the occurrence of in-phase and anti-phase oscillations. The full PDE–DDE system given by Eq. (1) and (2) is simulated by discretizing the PDE into a system of ODEs using a method of line approach with a spatial step size $h = 1/20$. The resulting ODE–DDE system is solved using the DDE solver dde23 in MATLAB. The amplitude plots and Floquet multipliers are computed for the DDE–ODE system using DDE-BIFTOOL.

First, suppose that the gain is $\beta = 1$ as in Fig. 1(a), (b). For $D = 0.1$ and the initial condition

$$C(x, t) = 1, \qquad X_1(t) = 1 + 0.1, \qquad X_2(t) = 1 - 0.1, \qquad -\tau \le t \le 0, \tag{21}$$

the numerical solution with different time delays is shown in Fig. 5(a), (b). We find that the primary Hopf bifurcation to an anti-phase solution is supercritical at the predicted critical time delay $\tau = \tau_{hp} \approx 1.99$ (see the inset of Fig. 1(a)). As τ increases to 2.3, although the in-phase oscillation is observed for the initial condition $X_1 = X_2 = 1.1$ (indicating that the blue curve in the inset of Fig. 1(a) has been crossed), we find that it is unstable for initial conditions that are not symmetric. For the sake of illustration, we choose the initial condition

$$C(x, t) = 1, \qquad X_1(t) = 1 + 0.1, \qquad X_2(t) = 1 + 0.09, \qquad -\tau \le t \le 0.$$

The numerical solution starts near an in-phase oscillation but evolves to an anti-phase oscillation, see Fig. 5(c). The instability of in-phase oscillations is also observed when we plot the amplitude of the periodic solutions using DDE-BIFTOOL, see Fig. 5(d). The stability is determined by computing the Floquet multipliers using DDE-BIFTOOL. We find that the in-phase oscillations have Floquet multipliers outside the unit circle. On the other hand, the anti-phase oscillations have Floquet multipliers inside the unit circle. Plotting the amplitude as a function of delay for $\beta = 1$ and fixed D corresponds to taking a vertical slice through Fig. 1(a).

Now, suppose that the diffusion coefficient is increased to $D = 0.6$. Consistent with Fig. 1(a), (b) we now find that the anti-phase oscillation is unstable and the in-phase oscillation is stable, see Fig. 6. This feature was also observed in the PDE–ODE model of Ref. [1]. More complex behavior can be obtained if the system operates close to the double-Hopf point in Fig. 1(a), as has also been found for a PDE–ODE system [2]. For example, if $D = 0.5$ then the anti-phase oscillation can change from unstable to stable as the time delay τ is increased from 2.7 to 2.9, see Fig. 7(b), (c). The numerical stability analysis of the anti-phase periodic solution suggests that there exists a pair of complex Floquet multipliers outside the unit circle for $\tau > \tau_{tr} \approx 2.8$, see Fig. 7(a). This implies there is a torus bifurcation near $(D, \tau) \approx (0.5, 2.8)$.

A change of oscillation modes is also observed when the diffusion coefficient changes for a fixed time delay. For $\tau = 3.2$, as the diffusion coefficient D changes from 0.1 to 0.6, the oscillation switches from anti-phase to in-phase, see Fig. 8. A similar result is observed for $\tau = 2.5$, as the diffusion coefficient D changes from 0.1 to 0.4, see Fig. 9.

4. Winding number argument

In this section, we use the winding number argument studied in [1] to count the number N_0 of roots of the characteristic Eq. (13) with $\mathrm{Re}\,\lambda > 0$. If $N_0 = 0$, then the steady state is linearly stable. Otherwise, it is linearly unstable. Moreover, there is a Hopf point if there exists a root on the imaginary axis. We start with the eigenvalue λ associated with the in-phase oscillation and consider the function

$$F(\lambda) = B(\lambda, \tau) + \sqrt{\lambda D}\tanh\left(\frac{L}{2}\sqrt{\frac{\lambda}{D}}\right) = \beta\left[1 - \frac{\beta}{\lambda + \beta + re^{-\lambda\tau}}\right] + \sqrt{\lambda D}\tanh\left(\frac{L}{2}\sqrt{\frac{\lambda}{D}}\right). \tag{22}$$

Recall that we are taking the primary branch of $\sqrt{\lambda}$, whilst the first term on the right-hand side is analytic except for a countable set

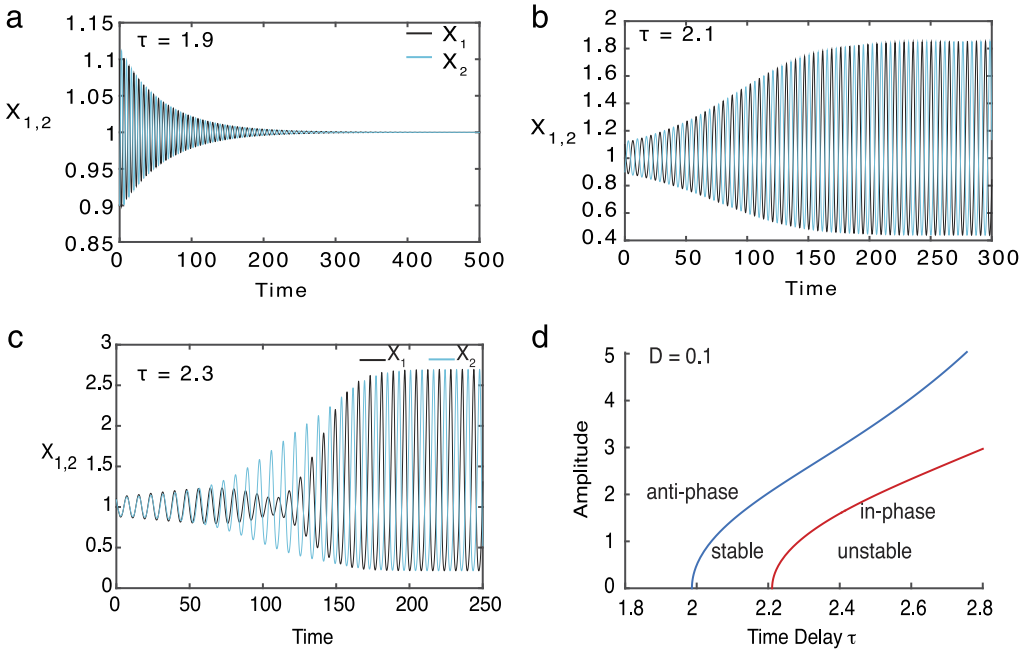

Fig. 5. Stable anti-phase solutions for $D = 0.1$, $\beta = 1.0$ and different delays τ. Corresponding bifurcation curves are shown in Fig. 1(a). (a) $\tau = 1.9$. The steady state solution is stable. (b) $\tau = 2.1$. Anti-phase oscillations occur given the initial condition $C(x, 0) = 1$, $X_1(0) = 1.1$, $X_2(0) = 0.9$. (c) $\tau = 2.3$. An in-phase oscillation changes to an anti-phase oscillation for the initial condition $C(x, 0) = 1$, $X_1(0) = 1.1$, $X_2(0) = 1.09$. (d) Amplitude of the periodic solutions as a function of time delay. Numerical result shows that the in-phase periodic solution has Floquet multipliers outside the unit circle and thus it is unstable. On the other hand, the anti-phase periodic solution has Floquet multiplier inside the unit circle. Other parameters: $L = 1$, $r = 1$, $M = 1$. Spatial step size $h = 0.05$.

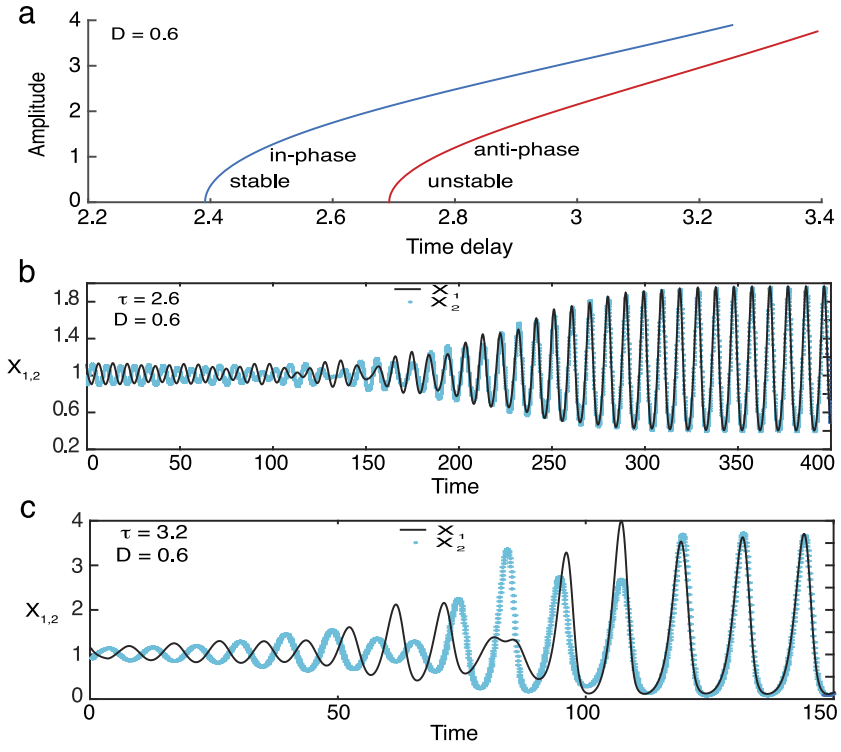

Fig. 6. Stable in-phase solutions for $D = 0.6$, $\beta = 1.0$ and different delays τ. Corresponding bifurcation curves are shown in Fig. 1(a). (a) Amplitude of the periodic solutions as a function of time delay. Numerical result shows that the anti-phase periodic solution has Floquet multipliers outside the unit circle and thus it is unstable. On the other hand, the in-phase periodic solution has Floquet multiplier inside the unit circle. (b, c) $\tau = 2.6,\ 3.2$, respectively. Initial condition: $C(x, 0) = 1$, $X_1(0) = 1.1, X_2(0) = 0.9$. Other parameters are $L = 1$, $r = 1$, $M = 1$.

of simple poles when $D > 0$. Replacing the tanh function by coth gives the eigenvalue λ associated with the anti-phase oscillation. To find the number of roots of F on the right-half complex plane $\{z, Re(z) > 0\}$, we construct the counterclockwise contour Γ consisting of the semi-circle $\Gamma_R = \{z = Re^{i\theta}, -\pi/2 < \theta < \pi/2\}$ and the imaginary axis $\Gamma_I = \{z = iy, -R \leq y \leq R\}$, see

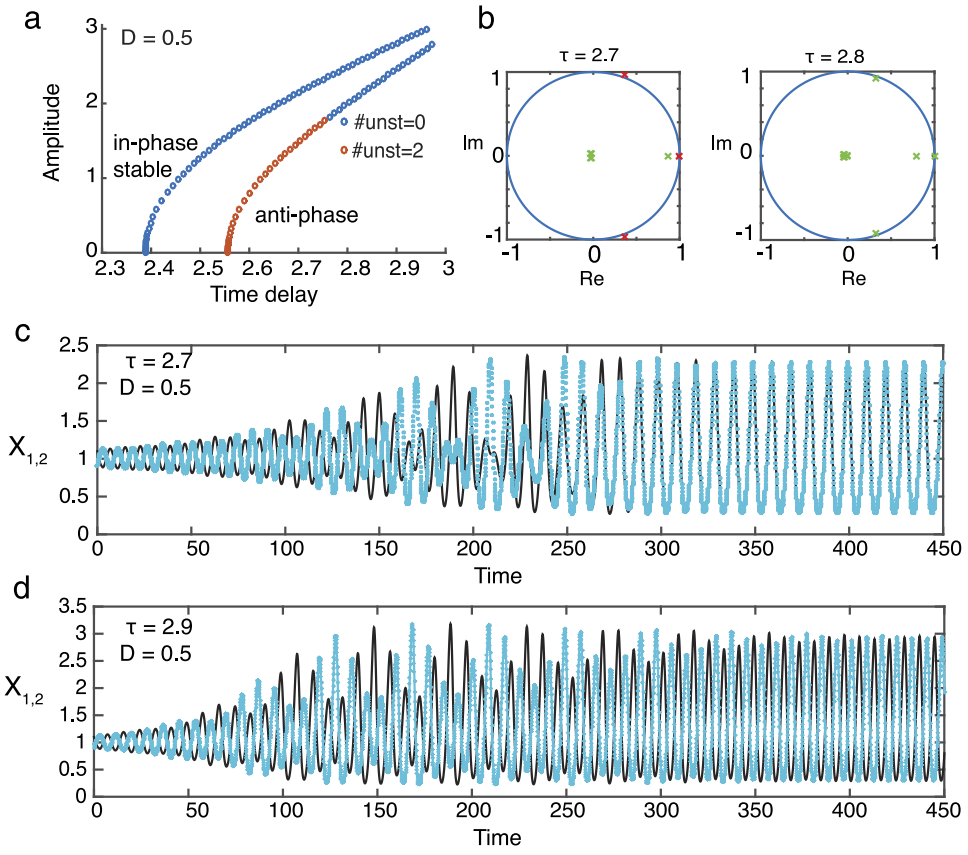

Fig. 7. Stability of the anti-phase oscillation for $D = 0.5$ and sufficiently large time delay. (a) Amplitude of the periodic solutions with the number of unstable Floquet multipliers. Blue: number of unstable Floquet multiplier (# unst) $= 0$, Red: number of unstable Floquet multiplier (# unst) $= 2$. (b) Plots of Floquet multipliers (anti-phase branch) with $\tau = 2.7$ and $\tau = 2.8$. There are a pair of complex Floquet multipliers (red markers) outside the unit circle for $\tau = 2.7$. (c) For $\tau = 2.7$, the anti-phase oscillation is unstable. (d) For $\tau = 2.9$, the anti-phase oscillation is stable. Initial condition: $C(x, 0) = 1$, $X_1(0) = 1.1, X_2(0) = 0.9$. Other parameters: $L = 1$, $\beta = 1$, $r = 1$, $M = 1$. (For interpretation of the references to color in this figure legend, the reader is referred to the web version of this article.)

Fig. 10. Applying the argument principle to the function $F(\lambda)$ on the contour Γ gives

$$N_0 - N_\infty = \frac{1}{2\pi}\Delta_\Gamma ArgF(\lambda), \tag{23}$$

where $N_0(N_\infty)$ is the number of zeros (poles) of F inside Γ and $\Delta_\Gamma ArgF(\lambda)$ is the change of the argument of F along the contour Γ. In the following, we perform the classical analysis to calculate N_∞ and $\Delta_\Gamma ArgF(\lambda)$ and determine N_0.

For the path Γ_R, as $R = |\lambda| \to \infty$, we have

$$|B(\lambda,\tau)| = \beta\left|1 - \frac{\beta}{\lambda+\beta+re^{-\lambda\tau}}\right| \le \beta + \frac{\beta^2}{|\lambda|-\beta-r} = \beta + O\left(\frac{1}{R}\right), \quad Re(\lambda) > 0,$$

and

$$\sqrt{\lambda D}\tanh\left(\frac{L}{2}\sqrt{\frac{\lambda}{D}}\right) \approx \sqrt{\lambda D}.$$

Hence

$$F(\lambda) \approx \beta + \sqrt{\lambda D} \Rightarrow |F(\lambda)| \approx \sqrt{RD} \neq 0, \quad \text{for } |\lambda| = R \gg 1. \tag{24}$$

So there are no zeros nor poles on Γ_R. Furthermore, we have

$$\Delta_{\Gamma_R} ArgF(\lambda) = ArgF(iR) - ArgF(-iR) = 2[ArgF(iR) - ArgF(0)] \approx \frac{\pi}{2}, \quad R \gg 1. \tag{25}$$

It follows that

$$\begin{aligned} N_0 &= N_\infty + \frac{1}{2\pi}\Delta_{\Gamma_R} ArgF(\lambda) + \frac{1}{2\pi}\Delta_{\Gamma_I} ArgF(\lambda) \\ &= N_\infty + \frac{1}{4} + \frac{1}{2\pi}\Delta_{\Gamma_I} ArgF(\lambda) \\ &= N_\infty + \frac{1}{4} + \frac{1}{\pi}\Delta_{\Gamma_I^+} ArgF(\lambda) \end{aligned} \tag{26}$$

where $\Gamma_{I^+} = \{z = iy, 0 \le y \le R\}$. It remains to calculate $\Delta_{\Gamma_I^+} ArgF(\lambda)$. Noting that

$$F(iR) \approx \sqrt{iDR} = \sqrt{DR}e^{i\pi/4}, \qquad F(0) = \frac{\beta r}{\beta + r} > 0, \tag{27}$$

the change of argument along the half imaginary axis Γ_{I^+} can be $\pi/4 + 2k\pi$ or $-\pi/4 + 2k\pi$. In Fig. 11, we sketch some possible images of $F(\Gamma_{I^+})$. For a given set of parameter values, we need to determine numerically whether or not the image $F(\Gamma_{I^+})$ crosses the negative real axis, and if it does then the number of times it crosses.

We also need to check if there are any poles or zeros on the path Γ_I. The number of poles or zeros is dependent on the parameters (β, τ, r). Note that if $F(\lambda)$ has a zero $\lambda = iy$, then there is a Hopf bifurcation. Since we are interested in the parameter regime above the Hopf curve, where an oscillatory solution has already emerged, we choose parameters so that there are no zeros on the imaginary axis. It can be checked that F has a pole where $B(\lambda, \tau)$ is singular. That is, $B(\lambda, \tau)$ has a pole on the imaginary axis Γ_I if there exists $\lambda = iy$ such that

$$H(\lambda) = \lambda + \beta + re^{-\lambda\tau} = 0. \tag{28}$$

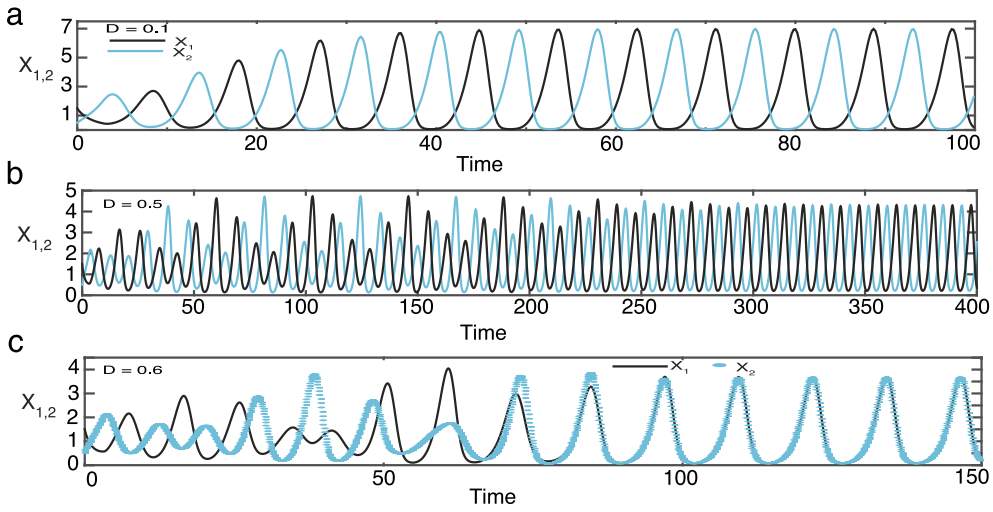

Fig. 8. Switch from an anti-phase oscillation to an in-phase oscillation as D increases from 0.1 to 0.6 with a fixed time delay $\tau = 3.2$. (a) $D = 0.1$, (b) $D = 0.5$, (c) $D = 0.6$. As the diffusion coefficient increases from 0.1 to 0.6, the solution changes from anti-phase oscillations to in-phase oscillations, see (a) and (c). For $D = 0.5$, a new type of oscillatory mode (torus) emerges due to the double Hopf bifurcation. However, the new mode disappears at a sufficiently large time ($t \approx 300$, see (b)), and the oscillations are again anti-phase. For $D = 0.6$, the oscillation starts as anti-phase but ends up as in-phase. Initial conditions: $C(x, 0) = 1,\ X_1(0) = 1.5, X_2(0) = 0.5$.

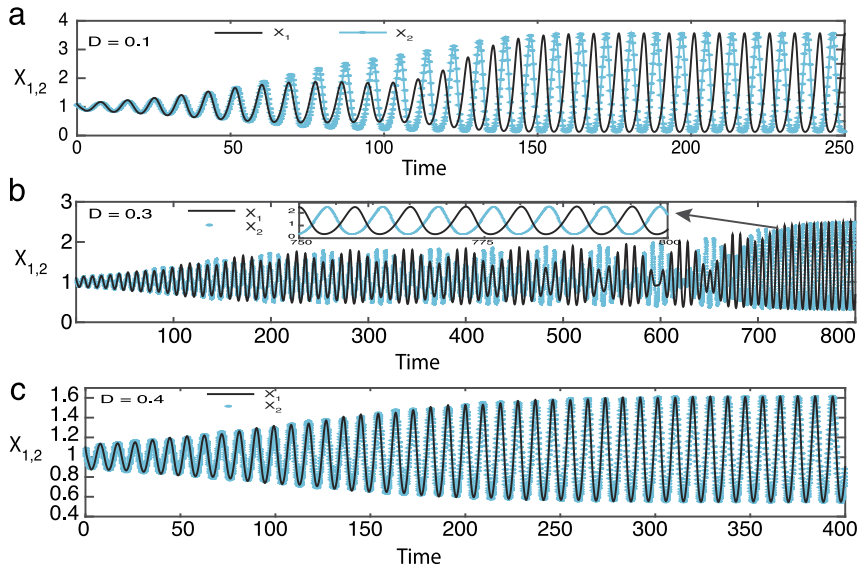

Fig. 9. As in Fig. 8, a switch in oscillation mode occurs when D increases from 0.1 to 0.4 with a fixed time delay $\tau = 2.5$. Initial conditions: $C(x, 0) = 1,\ X_1(0) = 1.1, X_2(0) = 1.09$.

Setting $\lambda = iy$ and separating the imaginary and real parts of $H(\lambda)$ gives

$$y - r\sin(y\tau) = 0, \tag{29a}$$
$$\beta + r\cos(y\tau) = 0. \tag{29b}$$

It follows that $\cos(y\tau) = -\beta/r$ and $\sin(y\tau) = \pm\sqrt{1-\beta^2/r^2}$. Note that if $r < \beta$, there is no solution of y to Eq. (29b). That is, there are no poles on Γ_l provided $r < \beta$.

If $r \geq \beta$, we can eliminate y from Eq. (29b) using $y = r\sin(y\tau) = \pm r\sqrt{1-\beta^2/r^2}$. That is,

$$\beta + r\cos(\tau\sqrt{r^2-\beta^2}) = 0. \tag{30}$$

For any fixed $\beta, \tau > 0$, and $r \geq \beta$, Eq. (30) has denumerably many positive solutions $\{r_i(\beta)\}$, see Fig. 15. For any $r \neq r_i(\beta)$, Eq. (30) does not have a solution, i.e., there is no zeros of $H(\lambda)$ on the imaginary axis. That is, there are no poles of F on Γ_l.

In order to find the number of poles N_∞ inside the contour Γ, we cite the Lemma 3 in [26].

Lemma 4.1 (*Hadeler and Tomiuk [26]*). *Let $\nu > 0$ be given. Then equation*

$$\nu + \alpha\cos\sqrt{\alpha^2-\nu^2} = 0$$

has denumerably many positive solutions

$$\alpha_1(\nu) < \alpha_2(\nu) < \alpha_3(\nu) < \cdots$$

with $\sin\sqrt{\alpha^2-\nu^2} > 0$, such that $\alpha_k(\nu) \to \infty$ as $k \to \infty$. For $\alpha \in (\alpha_k(\nu), \alpha_{k+1}(\nu)]$, equation

$$H(\lambda; \alpha, \nu) = \nu + \lambda + \alpha e^{-\lambda} = 0$$

has exactly k solutions $\lambda^1, \lambda^2, \ldots, \lambda^k$ in $Re\lambda > 0$, $Im\lambda > 0$, and

$$Re\lambda^l > 0, \qquad (2l - 3/2)\pi < Im\lambda^l < (2l-1)\pi, \quad l = 1, \ldots, k.$$

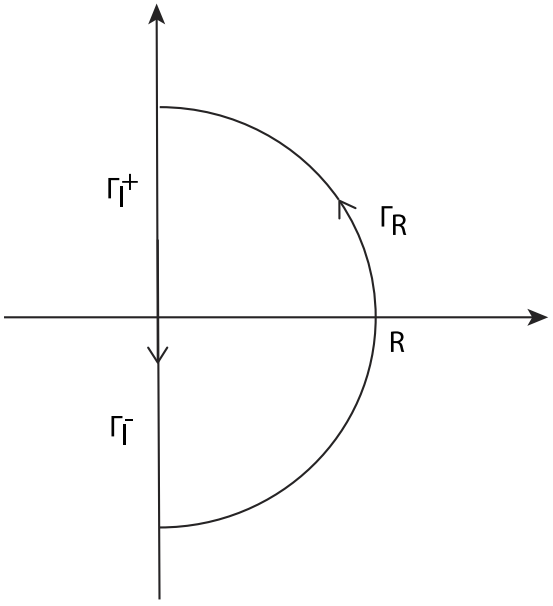

Fig. 10. Counterclockwise contour Γ consisting of the semi-circle $\Gamma_R = \{z = Re^{i\theta}, -\pi/2 < \theta < \pi/2\}$ and the imaginary axis $\Gamma_I = \Gamma_{I^-} \cup \Gamma_{I^+} = \{z = iy, -R \le y \le R\}$.

4.1. Winding number for $\beta \ge r$

Set $\alpha = r\tau$ and $\nu = \beta\tau$ in Lemma 4.1, if $\beta \ge r$, then there are no poles on Γ_I nor inside the contour Γ. That is

$$N_\infty = 0. \tag{31}$$

In the particular case $D = \beta = r = 1$, the critical time delay (in-phase) is $\tau_{hp} \approx 2.436$. For $\tau = 2.3 < \tau_{\rm hp}$ and $\tau = 2.5 > \tau_{\rm hp}$, we plot $\mathrm{Re}F(iy)$ and $\mathrm{Im}F(iy)$ in Fig. 12. It follows from these plots that

$$N_0 = \frac{1}{4} + \frac{1}{\pi}\Delta_{\Gamma_I^+} ArgF(\lambda) = \begin{cases} \frac{1}{4} - \frac{1}{4} = 0, & \text{if } \tau = 2.3 < \tau_{hp}, \\ \frac{1}{4} + \frac{7}{4} = 2, & \text{if } \tau = 2.5 > \tau_{hp}. \end{cases} \tag{32}$$

Therefore, there are two eigenvalues associated with the in-phase oscillation in $Re\lambda > 0$ when $\tau > \tau_{hp}$. This holds until τ is further increased to the continuation of the anti-phase Hopf curve, see Fig. 1(a). A similar result for the eigenvalues associated with the anti-phase oscillation is shown in Fig. 13. The critical time delay (anti-phase) is $\tau_{hp} \approx 3.15$. Finally, in Fig. 14, we plot the real parts of the eigenvalues associated with the in-phase and anti-phase mode for different D and τ. We see that for a diffusion coefficient $D \ge 0.3$ and sufficiently large time delay, the eigenvalue corresponding to the synchronous mode has a larger positive real part, indicating that it is the dominant mode. This indicates that for an arbitrary perturbation near the steady-state we would expect to see in-phase oscillations for most initial conditions.

4.2. Winding number for $\beta < r$

Following from Lemma 4.1, for any $\beta > 0$ and $r \in (r_k(\beta), r_{k+1}(\beta)]$, fixed, there are k solutions in $Re\lambda > 0, Im\lambda > 0$. Here, $\{r_k(\beta)\}_k$ are solutions to Eq. (30), see Fig. 15. Since the conjugate $\bar\lambda$ is also an eigenvalue, it follows that

$$N_\infty = 2k, \quad \text{for } r \in (r_k(\beta), r_{k+1}(\beta)],\ k = 0, 1, 2, \ldots. \tag{33}$$

For simplicity, we will focus on the parameter regime with $r \le r_2$, for which the number of poles is

$$N_\infty = \begin{cases} 0, & \text{if } r \in (0, r_1(\beta)], \\ 2, & \text{if } r \in (r_1(\beta), r_2(\beta)]. \end{cases} \tag{34}$$

For the sake of illustration, suppose that $\beta = 0.6, \tau = 3$. We find that there are two types of critical values of r:

(1) the critical value at a Hopf point of F occurs at $r_{\rm hp} \approx 0.81$. If $r < r_{\rm hp}$, then the eigenvalue has negative real part and the steady state is linearly stable.
(2) the first two positive solutions of Eq. (30): $r_1 \approx 0.96$ and $r_2 \approx 1.56$. If $0 < r < r_1$, there are no poles inside the contour Γ, i.e., $N_\infty = 0$; whereas if $r_1 < r < r_2$, there are two poles in conjugate pairs, i.e., $N_\infty = 2$.

For $0 < r < r_{\rm hp}$, $r_{\rm hp} < r < r_1$ and $r_1 < r < r_2$, we plot the real and imaginary part of F in Fig. 16. The numerical result suggests

$$\Delta_{\Gamma_I^+} ArgF(\lambda) = \begin{cases} -\frac{\pi}{4}, & \text{if } r \in (0, r_{\rm hp}), \\ \frac{7\pi}{4}, & \text{if } r \in (r_{\rm hp}, r_1), \\ -\frac{\pi}{4}, & \text{if } r \in (r_1, r_2). \end{cases}$$

Hence the formula of the Argument Principle (26) gives

$$\begin{aligned} N_0 &= N_\infty + \frac{1}{4} + \frac{1}{\pi}\Delta_{\Gamma_I^+} ArgF(\lambda) \\ &= \begin{cases} 0 + \frac{1}{4} - \frac{1}{4} = 0, & \text{if } r \in (0, r_{\rm hp}), \\ 0 + \frac{1}{4} + \frac{7}{4} = 2, & \text{if } r \in (r_{\rm hp}, r_1), \\ 2 + \frac{1}{4} - \frac{1}{4} = 2, & \text{if } r \in (r_1, r_2). \end{cases} \end{aligned} \tag{35}$$

The numerical result suggests that for the parameter r above the Hopf curve in (β, r) plane, see Fig. 17, and $r \in [r_{\rm hp}, r_2]$, there are two eigenvalues with positive real parts. For $r = 0.9, 1$, the eigenvalues are $\lambda = 0.058 \pm 0.6i, 0.029 \pm 0.588i$, respectively.

5. Extensions of the analysis

So far we have focused on one example of a DDE, the delayed logistic equation, and assumed that the coupling between each compartment and the bulk is the same (symmetric coupling). In this section, we briefly explore extensions of our analysis to (a) asymmetric coupling and (b) a PDE–DDE model based on the Mackey–Glass equation [15]. In the latter case, we show that most of our results still hold, but that the dominant mode for large D is now the anti-phase solution rather than the in-phase solution.

5.1. Asymmetric coupling

Let β_1 and β_2 denote the diffusive coupling between the two compartments and the bulk. In previous sections, we took $\beta_1 = \beta_2 = \beta$ (symmetric coupling). Here, we briefly explore what happens in the case of asymmetric coupling, $\beta_1 \ne \beta_2$, see also section 5 of [1]. Eq. (1) and (2) become

$$\begin{aligned} &\frac{\partial C}{\partial t}(x,t) = D\frac{\partial^2 C}{\partial x^2}, \quad 0 < x < L,\ t > 0 \\ &D\partial_x C(0,t) = \beta_1(C(0,t) - X_1(t)), \\ &-D\partial_x C(L,t) = \beta_2(C(L,t) - X_2(t)) \end{aligned} \tag{36}$$

and

$$\frac{dX_1}{dt}(t) = \beta_1(C(0,t) - X_1(t)) + f(X_1(t), X_1(t-\tau)), \tag{37a}$$

$$\frac{dX_2}{dt}(t) = \beta_2(C(L,t) - X_2(t)) + f(X_2(t), X_2(t-\tau)). \tag{37b}$$

It can be checked that the nonnegative steady-state solutions are $X_1 = X_2 = C(x) = 0$ and $X_1 = X_2 = C(x) = 1$. Although the steady-state solution is the same as the case when $\beta_1 = \beta_2$,

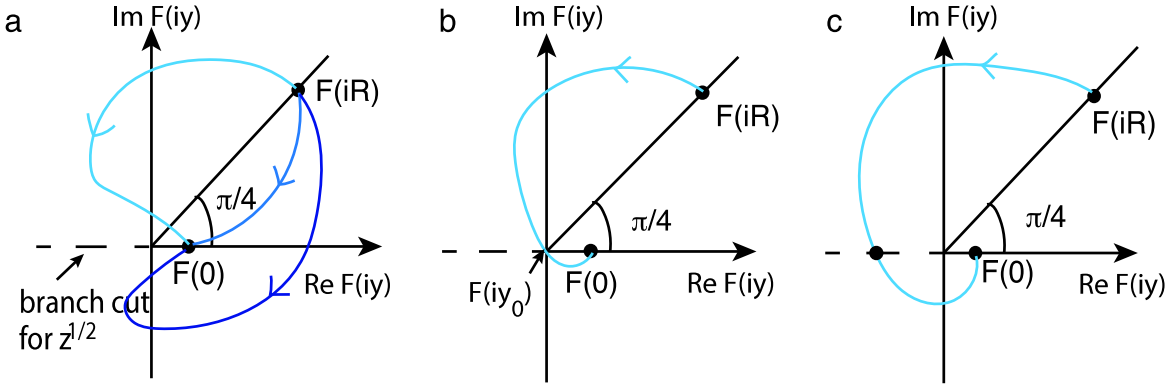

Fig. 11. Sketch of possible trajectories of $F(iy)$ as y changes from R to 0. (a) Three examples of trajectories that do not pass through the negative real axis and $\Delta ArgF = 0-\pi/4$. (b) Hopf bifurcation. There exists a $y_0 \in (0, R)$ such that $F(iy_0) = 0$. (c) $F(iy)$ crosses the negative real x-axis, $\Delta_{\Gamma_{1^+}} ArgF = (\pi - \pi/4) + 0 - (-\pi) = 7\pi/4$. Noting that the square root function does not appear in the function $B(iy, \tau)$, it is possible that $F(iy)$ crosses the negative x-axis.

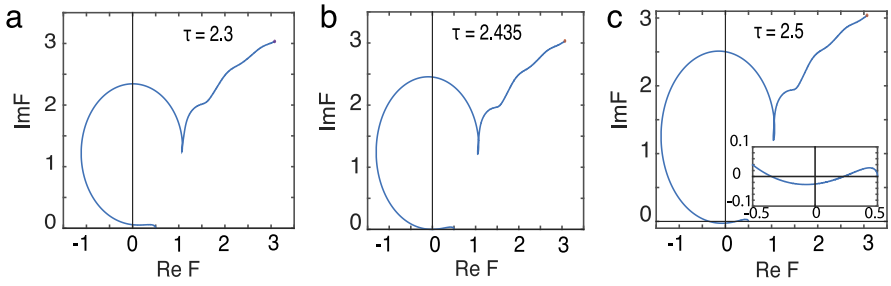

Fig. 12. Numerical plots of $F(iy)$ (in-phase) as y changes from R to 0 for different values of the delay τ. (a) Below the Hopf point. $\tau = 2.3 < \tau_{hp}$, $\Delta_{\Gamma_{1^+}} ArgF = -\pi/4$. (b) $\tau = \tau_{hp} = 2.435$. (c) $\tau = 2.5 > \tau_{hp}$, $\Delta_{\Gamma_{1^+}} ArgF = 7\pi/4$. Other parameters: $L = 1,\ D = 1,\ \beta = 1,\ r = 1,\ M = 1,\ R = 10$.

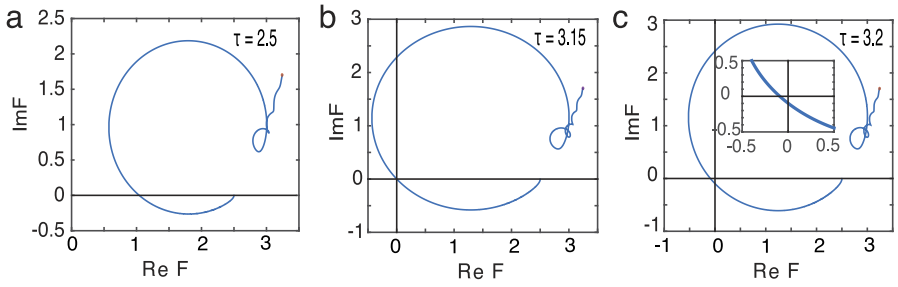

Fig. 13. Numerical plots of $F(iy)$ (anti-phase) as y changes from R to 0 for different values of the delay τ. (a) $\tau = 2.5 < \tau_{hp}$, $\Delta_{\Gamma_{1^+}} ArgF = -\pi/4$. $Re(F) > 0$. (b) $\tau = \tau_{hp} = 3.15$. (c) $\tau = 3.2 > \tau_{hp}$, $\Delta_{\Gamma_{1^+}} ArgF = 7\pi/4$. Other parameters: $L = 1,\ D = 1,\ \beta = 1,\ r = 1,\ M = 1,\ R = 10$.

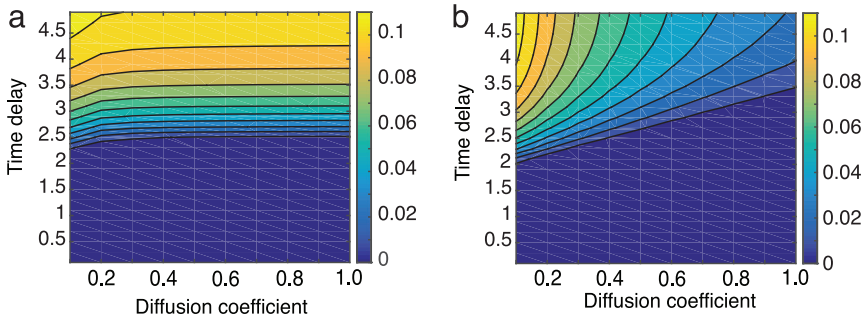

Fig. 14. Contour plots of $\max(\Re(\lambda), 0)$ in the (D, τ) plane with $D \in [0.1, 1]$ and $\tau \in [0, 5]$. (a) Eigenvalues of in-phase mode. (b) Eigenvalues of anti-phase mode. The numerical results indicate that for a diffusion coefficient $D \geq 0.3$ and sufficiently large time delay, the eigenvalue corresponding to the synchronous or in-phase mode has a larger positive real part. Parameters: $L = 1,\ \beta = 1,\ r = 1,\ M = 1$.

the amplitude and phase of the oscillations at the two end compartments are sensitive to the coupling parameters β_1 and β_2, see Fig. 18. For asymmetric coupling, the two oscillators are less likely to be synchronized. Firstly, the phases of the solutions can be different. Secondly, the weakly coupled oscillator has a relatively larger amplitude, see Fig. 18(a), (b), (d) and Fig. 11 of Ref. [1]. The difference of the amplitudes decreases when the asymmetry of the two coupling strengths gets smaller, see Fig. 18(a), (b).

To explore the effect of asymmetric coupling on the Hopf bifurcation, we take $\beta_2 = 1$ and plot the Hopf bifurcation curves

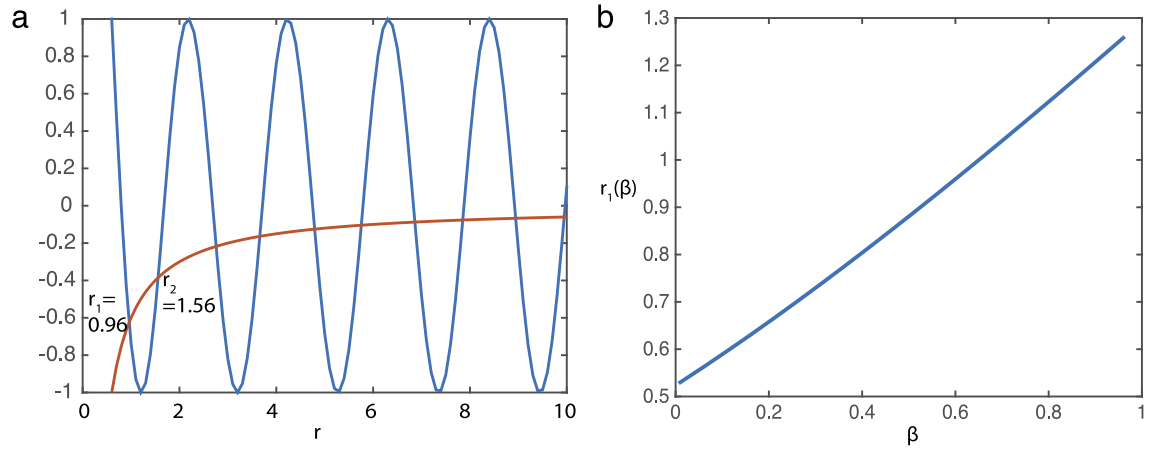

Fig. 15. (a) Plot of $\cos(\tau\sqrt{r^2-\beta^2})$ (blue) and $-\beta/r$ (red) as a function of r. As r increased from β to ∞, these two functions intersect many times at $r = r_i(\beta)$, $i \in \mathbb{N}$. (b) the smallest positive solution $r_1(\beta)$ as a function of β. For the parameter (β, r) lies below the curve, there is no zeros of $H(\lambda) = \lambda + \beta + re^{-\lambda\tau}$ on the right half plane. Baseline parameters $\beta = 0.6,\ \tau = 3$. (For interpretation of the references to color in this figure legend, the reader is referred to the web version of this article.)

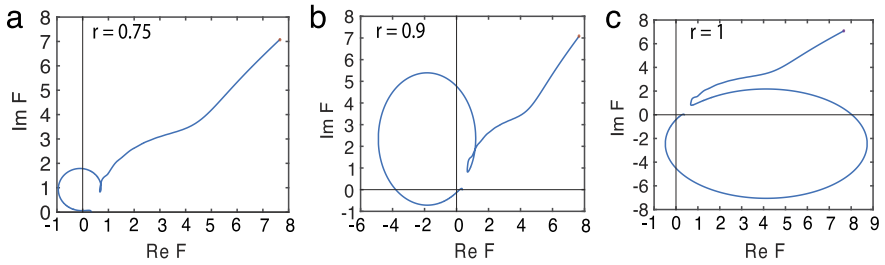

Fig. 16. $ReF(\lambda)$ and $ImF(\lambda)$ as λ travels along $\Gamma_{I^+} = \{iy\}$ with y changes from 100 to 0.01. (a) $r = 0.75 < r_{hp} = 0.81$. Since $ImF > 0$, we have $\Delta_{\Gamma_{I^+}} = -\pi/4$. (b) $r = 0.9 \in (r_{hp}, r_1)$, $\Delta_{\Gamma_{I^+}} = 7\pi/4$. (c) $r = 1 \in (r_1, r_2)$, $\Delta_{\Gamma_{I^+}} = -\pi/4$. Other parameters: $\beta = 0.6,\ \tau = 3,\ D = 1,\ L = 1,\ R = 100$.

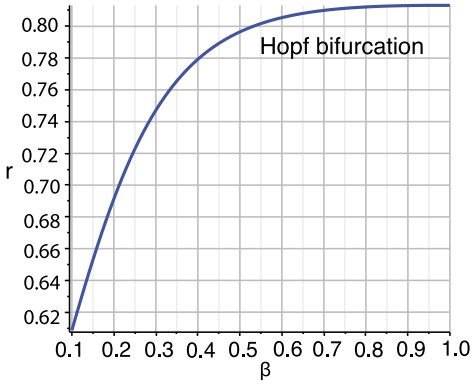

Fig. 17. Hopf bifurcation in (β, r) plane. Parameters $D = 1,\ \tau = 3,\ L = 1$.

in the (β_1, τ) plane for different values of D in Fig. 19. For $D = 0.2$ and $D = 0.3$, there are two Hopf branches, which have different limiting values of time delay as β_1 goes to 0, see Fig. 19(a). As $\beta_1 \to 0$, the Hopf bifurcation curve (blue) has the critical time delay $\tau \to \pi/2$ which is the critical time delay of the delayed logistic equation. This suggests that diffusion has a weak effect on the time delay of the weakly coupled compartment X_1. As $\beta_1 \to 0$, the time delay on the second Hopf branch (dashed green line) is the same as the critical time delay of the model given by Eq. (36) and (37) with $\beta_1 = 0$. The two Hopf branches separate the (β_1, τ) plane into three different regions, see Fig. 19(a). In region 1, below the Hopf curve, the steady state solution is stable. In region 2, above the Hopf curve, the steady state solution is unstable and there are periodic solutions of $X_{1,2}$ with different phases and amplitudes. For the sake of illustration, we take $\beta_1 = 0.1$, and plot the numerical solution with time delay below or above the critical time delay in Fig. 19(c), (d). In region 3, there exist an in-phase oscillation and oscillations with different phases, see Fig. 18(b), (c). In particular, the in-phase oscillation occurs when $\beta_1 = \beta_2$.

In Fig. 20, we compare the numerical solutions for $\beta_1 < \beta_2$ and $\beta_1 = \beta_2$. For $\beta_1 = \beta_2$, if τ is below the second Hopf branch, then the numerical solution with initial condition $X_1 = X_2$ converges to the steady state; if τ is above the second Hopf branch, then the solution changes to periodic solutions with different phases, see Fig. 20(a), (b). For $\beta_1 < \beta_2$, the numerical solution of $X_{1,2}$ starts with the same phase and amplitude but ends up with different phases and amplitudes, see Fig. 20(c), (d).

5.2. PDE coupled with the Mackey–Glass equation

In this section, we replace the delay Logistic equation (3) by another classical delay differential equation, namely, the Mackey–Glass equation [15]. Let

$$f(x(t), x(t-\tau)) = a_1 \frac{x(t-\tau)}{1 + x^n(t-\tau)} - a_2 x(t). \tag{38}$$

If $a_2/a_1 > 1$, then f has a positive solution at

$$x = \sqrt[n]{a_1/a_2 - 1}.$$

Suppose that we set $a_2 = 1$. Example Hopf bifurcation curves of the Mackey–Glass equation

$$\frac{dX}{dt} = a_1 \frac{X(t-\tau)}{1 + X^n(t-\tau)} - a_2 X(t)$$

are shown Fig. 21(a). For both $n = 10$ and $n = 15$, the critical time delay decreases as a_1 increases. For $a_1 = 2$ and $n = 10, 15$, the critical time delay is $\tau \approx 0.47, 0.27$, respectively.

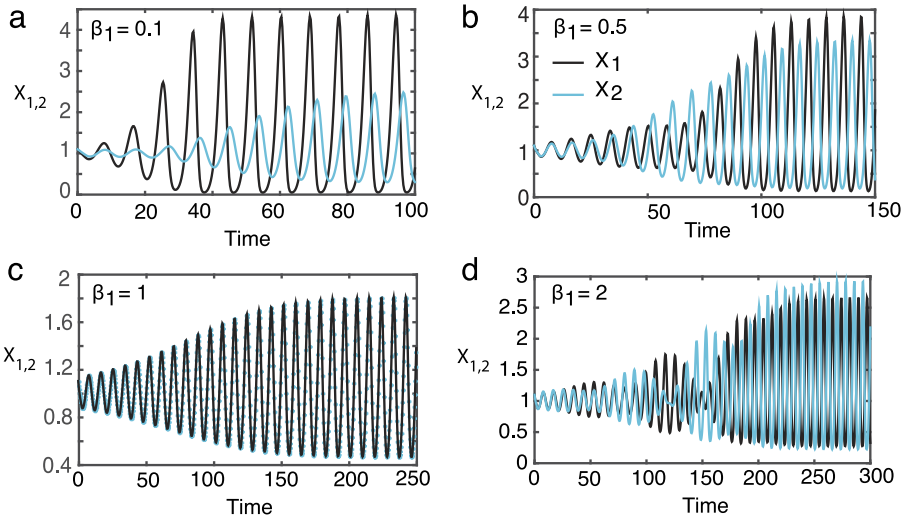

Fig. 18. Change of the phase and amplitude of the oscillations with different values of the coupling parameter β_1. The other coupling parameter β_2 is fixed to be 1. (a, b) $\beta_1 = 0.1$ and $\beta_1 = 0.5$. The oscillator with a weaker coupling has a larger amplitude. The difference between the amplitudes becomes smaller as β_1 increased from 0.1 to 0.5. (c) Symmetric coupling $\beta_1 = \beta_2$. The two oscillators have the same amplitude and phase. (d) Strongly coupled oscillators with $\beta_1 = 2$. The difference of the amplitude or phase is small when the coupling strength is strong at both ends. Initial condition: $X_1(t) = X_2(t) = 1.1$, $C(x, t) = 1$. Parameters: $D = 0.2$, $\tau = 2.5$, $\beta_2 = 1$. Other parameters are the same as in Fig. 1.

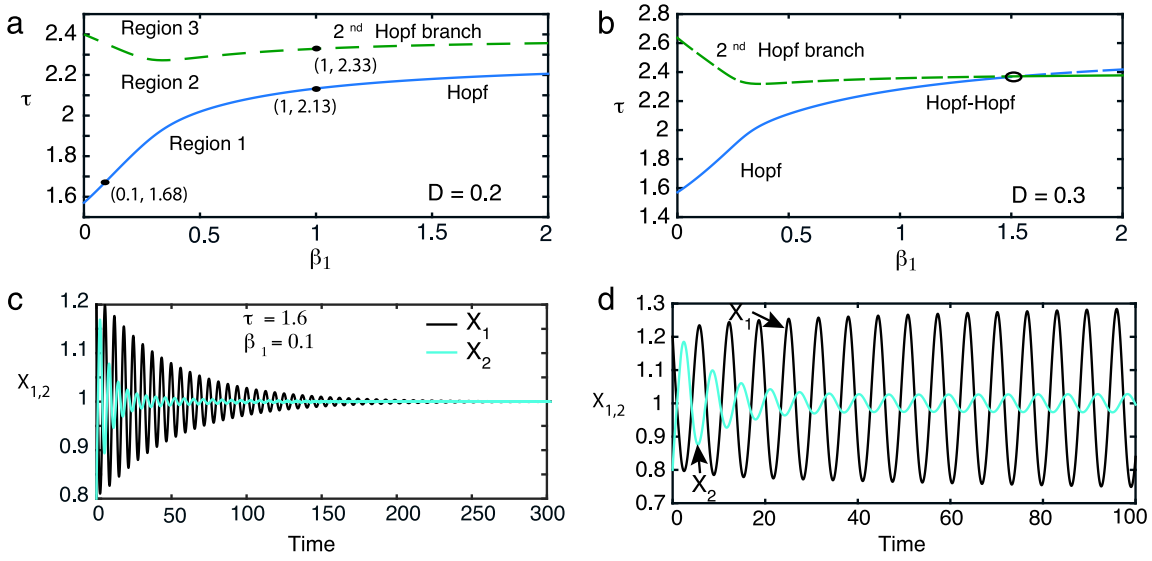

Fig. 19. Hopf bifurcation curves in the (β_1, τ) plane for $\beta_2 = 1$ and different D. (a) $D = 0.2$. There are three regions separated by the first two Hopf curves. In Region 1, the steady state is linearly stable. In Region 2, there are periodic solutions of $X_{1,2}(t)$ with different phases. In Region 3, when $\beta_1 = \beta_2$, there is an in-phase periodic solution, see Fig. 18(c). The first two Hopf branches do not intersect for $\beta_1 \in [0, 2]$. (b) Hopf bifurcation curves with $D = 0.3$. There is a Hopf–Hopf point. (c, d) Numerical solution with $D = 0.2$, $\beta_1 = 0.1$ and $\tau = 1.6$, 1.7, respectively. Initial condition: $X_1(t) = 1.2$, $X_2(t) = 0.8$, $C(x, t) = 1$. (For interpretation of the references to color in this figure legend, the reader is referred to the web version of this article.)

We then take $a_2 = 2$ and consider the full PDE-Mackey–Glass model (1)–(2) with f given by the Eq. (38). The Hopf bifurcation curves are plotted in Fig. 21(b), (c). The critical time delay increases as the diffusion coefficient increases, which is similar to our result of the PDE–Logistic model, see Fig. 1. On the other hand, in contrast to the PDE–Logistic equation, the mode of the oscillation emerging from a Hopf bifurcation is anti-phase rather than in-phase for a wide range of diffusion coefficients. This result suggests that the oscillation mode depends on the explicit form of the delay differential equations. For $D = 0.5$ and $n = 10$, the numerical solution with different time delays near the critical time delay $\tau_{hp} \approx 0.55$ is shown in Fig. 21(d)–(e). The existence of oscillation for $\tau = 0.57 > \tau_{hp}$ suggests that the Hopf bifurcation is supercritical. The oscillation modes are both anti-phase for $\tau = 0.57$ and $\tau = 0.6$. Although an in-phase oscillation is also observed for $\tau = 0.6$, we find that it is unstable with respect to perturbations near the initial condition $X_1 = X_2 = 1$.

6. Conclusions

In this paper, we analyzed a one-dimensional PDE–DDE model consisting of a pair of delayed logistic equations or Mackey–Glass equations coupled by one-dimensional bulk diffusion. We used linear stability analysis to derive the associated characteristic equation and then solved this equation numerically to plot the Hopf curves as a function of various model parameters. In the parameter regions above the Hopf bifurcation curves, our numerical results suggest that there are two different oscillation modes (reflecting the exchange symmetry of the system): in-phase and anti-phase. The selection of these modes is sensitive to

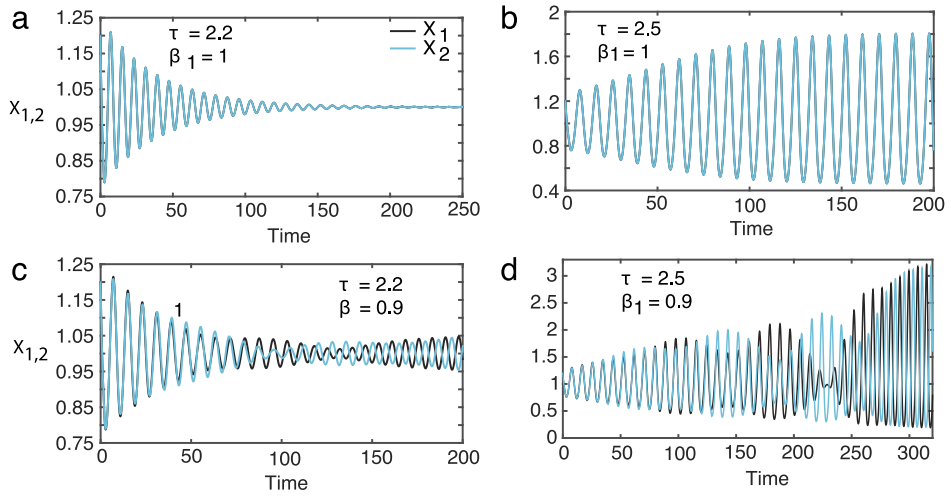

Fig. 20. Numerical solution with different τ and β_1 close to β_2. (a, b) $\beta_1 = \beta_2$ and $\tau = 2.2, 2.5$, respectively. The solution converges to the steady state for a smaller time delay $\tau = 2.2$ while it converges to a periodic solution(in-phase) for $\tau = 2.5$. The time delay $\tau = 2.2$ is below the time delay on the second Hopf branch, see Fig. 19(a). (c, d) $\beta_1 = 0.9 < \beta_2$ and $\tau = 2.2, 2.5$, respectively. The numerical solution of $X_{1,2}$ starts with the same phase and amplitude but ends up with different phases and amplitudes. Initial condition: $X_1(t) = X_2(t) = 1.2$ and $C(x, t) = 1$. Other parameters: $\beta_2 = 1,\ D = 0.2$.

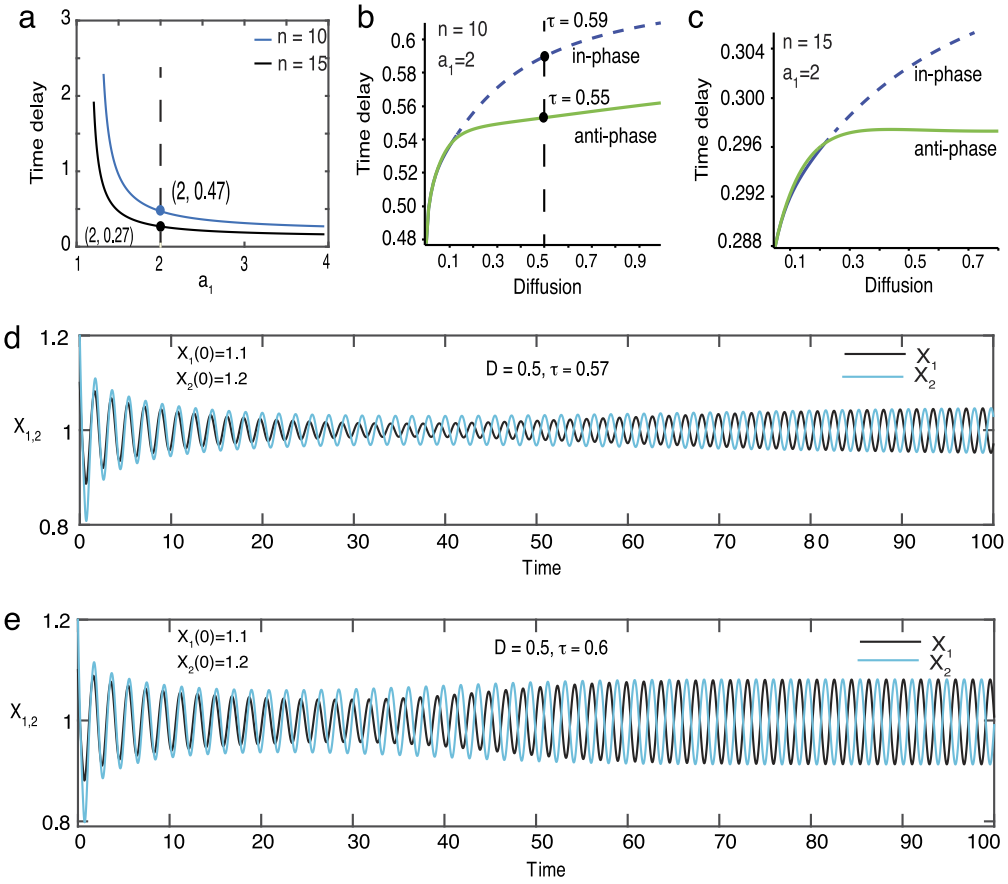

Fig. 21. Numerical result of PDE–DDE model with Mackey–Glass model. (a) Hopf bifurcation in (a_2, τ) plane with $n = 10, 15$. (b, c) Hopf bifurcation curves of the PDE-Mackey–Glass model in (D, τ) plane with $a_2 = 2$. (d, e) Numerical solution for $D = 0.5$ and $\tau = 0.57, 0.6$. Initial condition: $C(x, 0) = 1,\ X_1(0) = 1.1, X_2(0) = 1.2$. Other parameters: $a_1 = 2,\ a_2 = 1,\ \beta = 1,\ L = 1$.

the diffusion coefficient, the time delay and the explicit form of delayed feedback.

Certain care has to be taken in directly comparing our results to those of Gou et al. for one-dimensional PDE–ODE systems [1,2,4], since we do not include a degradation term in the bulk diffusion equation. Nevertheless, a number of similarities can be noted. First, both PDE–DDE and PDE–ODE systems support oscillations that can be in-phase or anti-phase. Second, the onset of oscillations and the selection between the two oscillation modes is sensitive to the value of the diffusion coefficient. In the PDE–DDE case without degradation, we found that increasing the diffusivity tends to stabilize the stead-state solution, thus delaying the onset of a Hopf bifurcation. On the other hand, for a PDE–ODE model with degradation and conditional oscillators [4], oscillations occur over

a bounded range of diffusivities that excludes $D = 0$, so that increasing D from zero can induce an oscillation. For the PDE–ODE models studied in Refs. [1,2,4], the in-phase solution tended to be dominant over a wide range of parameters. We also found this to be true in the case of the logistic delayed equation, but found the anti-phase solution to be dominant in the case of Mackey–Glass. Finally, both the PDE–DDE and PDE–ODE models exhibit parameter regimes where in-phase and anti-phase oscillations coexist due to the presence of a Hopf–Hopf bifurcation point, which also acts as the organizing center for more complex oscillations indicative of a torus bifurcation [3].

There are a number of issues worth further exploration. First, it would be interesting to carry out a more detailed study of the double Hopf bifurcation arising from the PDE–DDE model and to determine the basin of attractions of coexistent in-phase and anti-phase solutions, see also [3]. Second, in this paper, we considered a few common scalar DDEs to develop the basic theory. However, we are ultimately interested in understanding the effects of diffusive coupling on complex multi-species biochemical oscillators. As part of this, we would like to compare the behavior of the resulting PDE–ODE system to the corresponding PDE–DDE system, with the latter obtained by reducing each multi-component ODE by a DDE along the lines of Ref. [13].

References

[1] J. Gou, Y. Li, W. Nagata, M. Ward, Synchronized oscillatory dynamics for a 1-d model of membrane kinetics coupled by linear bulk diffusion, SIAM J. Appl. Dyn. Syst. 14 (4) (2015) 2096–2137.

[2] J. Gou, M. Ward, Oscillatory dynamics for a coupled membrane-bulk diffusion model with Fitzhugh–Nagumo membrane kinetics, SIAM J. Appl. Math. 76 (2) (2016) 776–804.

[3] J. Gou, Y.-X. Li, W. Nagata, Interaction of in-phase and anti-phase synchronies in a coupled compartment-bulk diffusion model at a double Hopf bifurcation, IMA J. Appl. (2016) (in press).

[4] J. Gou, W.-Y. Chiang, P.-Y. Lai, M.J. Ward, Y.-X. Li, A theory of synchrony by coupling through a diffusive chemical signal, Physica D (2016) (in press).

[5] A. Gomez-Marin, J. Garcia-Ojalvo, J.M. Sancho, Self-sustained spatiotemporal oscillations induced by membrane-bulk coupling, Phys. Rev. Lett. 98 (16) (2007) 168303.

[6] J. Gou, M. Ward, An asymptotic analysis of a 2-d model of dynamically active compartments coupled by bulk diffusion, J. Nonlinear Sci. (2016) 1–51.

[7] M.B. Miller, B.L. Bassler, Quorum sensing in bacteria, Annu. Rev. Microbiol. 55 (1) (2001) 165–199.

[8] J. Müller, C. Kuttler, B.A. Hense, M. Rothballer, A. Hartmann, Cell–cell communication by quorum sensing and dimension-reduction, J. Math. Biol. 53 (4) (2006) 672–702.

[9] J. Müller, H. Uecker, Approximating the dynamics of communicating cells in a diffusive medium by odes—homogenization with localization, J. Math. Biol. 67 (5) (2013) 1023–1065.

[10] W.-Y. Chiang, Y.-X. Li, P.-Y. Lai, Simple models for quorum sensing: Nonlinear dynamical analysis, Phys. Rev. E 84 (4) (2011) 041921.

[11] P.C. Bressloff, Ultrasensitivity and noise amplification in a model of v. harveyi quorum sensing, Phys. Rev. E 93 (2016) 062418.

[12] S.Y. Shvartsman, E. Shütz, R. Imbihl, I.G. Kevrekidis, Dynamics on microcomposite catalytic surfaces: the effect of active boundaries, Phys. Rev. Lett. 83 (14) (1999) 2857.

[13] B. Novak, J.J. Tyson, Design principles of biochemical oscillators, Nat. Rev. Mol. Cell Biol. (2008) 981–991.

[14] J. Wu, Theory and Applications of Partial Functional Differential Equations, Vol. 119, Springer Science & Business Media, 2012.

[15] M.C. Mackey, L. Glass, Oscillation and chaos in physiological control systems, Science 197 (1977) 287–289.

[16] J.K. Hale, S.M.V. Lunel, Introduction to Functional Differential Equations, Vol. 99, Springer Science & Business Media, 2013.

[17] Y. Kuang, Delay Differential Equations: With Applications in Population Dynamics, Vol. 191, Academic Press, 1993.

[18] H. Smith, An Introduction to Delay Differential Equations with Applications to the Life Sciences, Vol. 57, Springer Science & Business Media, 2010.

[19] N. MacDonald, Time Lags in Biological Models, Vol. 27, Springer Science & Business Media, 1978.

[20] S. Ruan, Delay differential equations in single species dynamics, in: Delay Differential Equations and Applications, Springer, 2006, pp. 477–517.

[21] J. Mahaffy, C. Pao, Models of genetic control by repression with time delays and spatial effects, J. Math. Biol. 20 (1) (1984) 39–57.

[22] S. Busenberg, J. Mahaffy, Interaction of spatial diffusion and delays in models of genetic control by repression, J. Math. Biol. 22 (3) (1985) 313–333.

[23] S. Busenberg, J. Mahaffy, The effects of dimension and size for a compartmental model of repression, SIAM J. Appl. Math. 48 (4) (1988) 882–903.

[24] K. Engelborghs, T. Luzyanina, D. Roose, Numerical bifurcation analysis of delay differential equations using dde-biftool, ACM Trans. Math. Software (TOMS) 28 (1) (2002) 1–21.

[25] B. Xu, P.C. Bressloff, A PDE-DDE model for cell polarization in fission yeast, SIAM J. Appl. Math. 76 (2016) 1844–1870.

[26] K. Hadeler, J. Tomiuk, Periodic solutions of difference-differential equations, Arch. Ration. Mech. Anal. 65 (1) (1977) 87–95.

[27] N. Hayes, Roots of the transcendental equation associated with a certain difference-differential equation, J. Lond. Math. Soc. 1 (3) (1950) 226–232.